Journal of Power Sources 255 (2014) 52–58

Contents lists available at ScienceDirect

Journal of Power Sources

journal homepage: www.elsevier.com/locate/jpowsour

Co_3O_4 mesoporous nanostructures@graphene membrane as an integrated anode for long-life lithium-ion batteries

Lu Li, Guangmin Zhou, Xu-Yi Shan, Songfeng Pei, Feng Li*, Hui-Ming Cheng

Shenyang National Laboratory for Materials Science, Institute of Metal Research, Chinese Academy of Sciences, 72 Wenhua Road, Shenyang 110016, China

HIGHLIGHTS

- A facile and large scale synthesis of integrated electrode materials is proposed.
- The light graphene current collector will increase the energy density of cell.
- Porous structure is beneficial for Li^+ transfer and strain buffer of Co_3O_4.
- Superior cycling performance without capacity loss over 500 cycles is obtained.

GRAPHICAL ABSTRACT

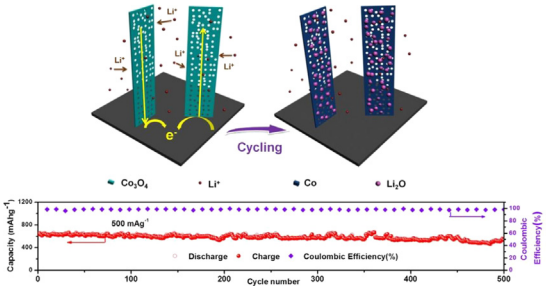

ARTICLE INFO

Article history:
Received 23 October 2013
Received in revised form
26 December 2013
Accepted 31 December 2013
Available online 8 January 2014

Keywords:
Mesoporous Co_3O_4
Controllable structures
Graphene membrane
Integrated anode
Lithium-ion batteries

ABSTRACT

One of the most attractive research areas in lithium-ion batteries (LIBs) is to design elaborate nanostructure of the electrode, which has been considered as keys to solve the problems such as the low energy density, slow lithium ion and electron transport, and the large volume change of electrode materials during cycling processes. Here, mesoporous Co_3O_4 with controllable structures was directly grown on a graphene membrane by hydrothermal reaction followed by annealing treatment, and used as an integrated anode in LIBs without using metallic current collector, binder and conductive additive. The light graphene membrane as current collector with high electrical conductivity and stability contributes to the high energy density of LIBs. A mesoporous structure with enough space is beneficial to lithium ion diffusion and strain buffer of Co_3O_4 during discharge/charge processes, rendering the electrodes high performance. The integrated electrode shows good rate capability and impressive cycling stability without capacity loss over 500 cycles under a high current density of 500 mA g^{-1}.

1. Introduction

The appearance of high-performance consumer electronic products requires the development of lithium-ion batteries (LIBs) with high energy density [1,2]. On the one hand, discovering new systems with high energy density is a feasible approach, for example, the explorations on Li–S or Li-air batteries [3,4]. On the other hand, the performance of LIBs could be improved significantly by designing the structure of the electrode through reducing inactive components in the electrode, which seems to be a more effective and simpler way.

Generally, an electrode in LIBs is comprised of active material (contributing the capacity), conductive additive (providing electrical contact between components of the electrode) and current collector (Al or Cu foils, supporting the electrode material and offering a continuous conductive pathway), and polymeric binder (supplying the physical adhesion between the active material, conductive additive and current collector) [5]. The gravimetric energy density of conventional LIBs is only 42–58% of their theoretical value, therefore, there is still a considerably large space for

* Corresponding author.
E-mail addresses: fli@imr.ac.cn, nanowormx@gmail.com (F. Li).

0378-7753/$ – see front matter © 2014 Elsevier B.V. All rights reserved.
http://dx.doi.org/10.1016/j.jpowsour.2013.12.129

further improvement, such as reducing the inactive components in the electrode, etc [6]. In addition to no contribution to the capacity, the inactive components, such as insulating binder, will offset the benefits of high capacity materials and introduce undesirable interface, resulting in performance degradation during charge and discharge processes [7,8]. For a metal current collector, due to the long-term contact with the corrosive electrolyte, localized pitting corrosion in Al and environment-assisted cracking in Cu occur, which bring potential instable factors to the whole electrochemical system [9]. Moreover, multi-functional electronic devices require an energy storage system to be lightweight, thin and flexible [10,11]. It is important to adopt high capacity materials, decrease the ratio of inactive ingredients, and replace heavy metallic current collectors with more stable and lighter materials. Along this direction, there have been several studies focused on the electrode structure design to improve the energy density of cell and attempted to develop flexible functional devices, for example, the direct growth of active materials on lightweight and flexible substrates is promising and has demonstrated their potential applications [12–15].

Co_3O_4 is a promising anode for LIBs because of its low cost, nontoxicity, good chemical stability and high theoretical capacity (890 mAh g^{-1}), which is almost two and a half times that of the graphite anode (372 mAh g^{-1}) [16,17]. But its low electronic conductivity, rapid capacity loss and poor capacity retention have hampered its practical use in LIBs [18–20]. The use of carbon-based nanocomposites, optimizing particle size of active materials, adjusting the nanostructures of Co_3O_4, providing more active sites, allowing good electrolyte permeability and quick electron and ion transport are needed to be considered to solve these intractable problems [16,21,22]. For example, design of unique nanostructured Co_3O_4 such as nanotube, [23] nanowire, [24] nanosheet, [25] nanocage, [26] and mesoporous structure [27] has been proposed as effective method to improve the properties of Co_3O_4 electrodes. However, achieving good rate capability and long cycling life of Co_3O_4 electrode material, keeping large reversible capacity accompanying with high Coulombic efficiency, still remains a great challenge. Graphene, as a two-dimensional (2D) conductive support, has opened new possibilities due to its lightweight, high electrical conductivity, superior mechanical flexibility, and chemical stability [4]. Here, we propose an integrated anode in which nanostructured Co_3O_4 grown on a graphene membrane without using metallic current collector, binder and conductive additive for LIBs, therefore the energy density of the battery can be enhanced greatly. The integrated electrode was fabricated by a two-step process: hydrothermal reaction (the crucial step that determines the morphologies of nanostructured Co_3O_4) and annealing treatment (Fig. 1). Owing to the mesoporous structure which offers strain buffering space for Co_3O_4 and forms fast ions transport channels for Li^+ ion insertion, it provides more interface for lithium storage and the electrolyte is prone to diffuse to those active sites. Co_3O_4 directly grown on the graphene membrane with good electronic contact between graphene current collector and Co_3O_4 can facilitate electron transport [14]. The integrated electrode shows good rate capability and cycling stability without capacity loss over 500 cycles.

2. Experimental sections and characterizations

2.1. Synthesis of the graphene membrane

The graphene material used was obtained from Sichuan Jinlu Group, China, using a patent invented by our group [28]. The graphene membrane was fabricated by a vacuum-filtration and peeling-off process. Typically, the graphene material was dispersed in alcohol to form a suspension with a concentration of 0.2 mg mL^{-1}. The suspension was subsequently vacuum filtered using a Nylon membrane with a pore size of 0.44 μm. After fully drying at 90 °C for 30 min, the graphene membrane could be easily peeled off from the filter surface. The thickness of the graphene membrane is about 20 μm with a conductivity of 1000 S cm^{-1}, much higher than the reported chemically exfoliated or reduced graphene oxide film [15,29].

2.2. Synthesis of nanostructured Co_3O_4@graphene membrane

A hydrothermal process was used to tune the structure of Co_3O_4 on the graphene membrane. First, 0.582 g $Co(NO_3)_2 \cdot 6H_2O$ and 0.6 g $CO(NH_2)_2$ were dissolved in 50 mL de-ionized water, mixed and stirred for 10 min. The obtained homogeneous solution was transferred and sealed in an 80 mL Teflon-lined autoclave. A graphene membrane was soaked and floated in the solution. The

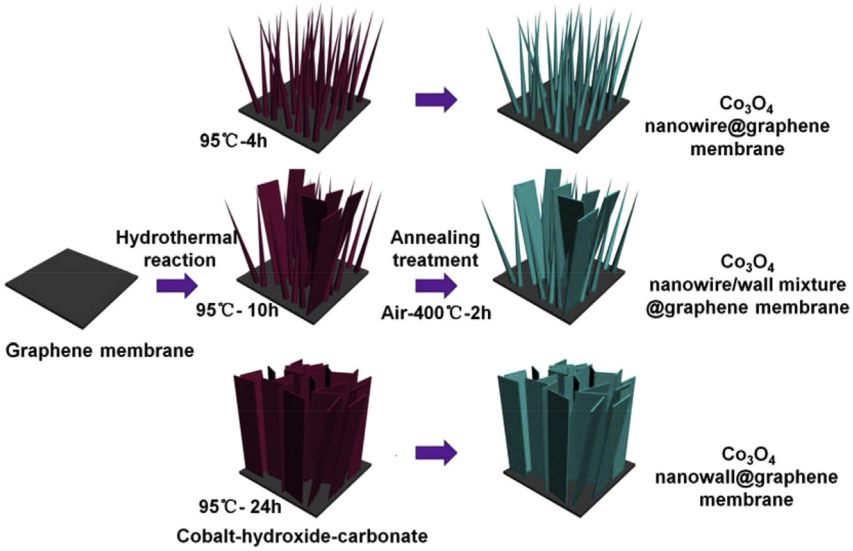

Fig. 1. Fabrication process of nanostructured Co_3O_4 grown on a graphene membrane.

autoclave was sealed, kept at 95 °C for 4–24 h, and cooled to room temperature naturally. The graphene membrane with light-pink deposit (cobalt-hydroxide-carbonate) [22] was washed with deionized water and alcohol, and dried at 50 °C. Finally, the sample was heated in air at 400 °C for 2 h to obtain nanostructured Co_3O_4@graphene membrane.

2.3. Synthesis of the pure Co_3O_4

Co_3O_4 sample was synthesized under the same conditions as that of Co_3O_4@graphene membrane but without adding the graphene membrane.

2.4. Characterization

X-ray diffraction (XRD) data were collected using D-MAX/2400 (Cu K*a*). The morphology, composition and structure of the samples were characterized by transmission electron microscopy (TEM) (Tecnai F20, 200 kV), scanning electron microscopy (SEM) (FEI Nova NanoSEM 430, 15 kV). Thermogravimetric (TG) measurements were carried out on a Netzsch-STA 449C, measured from 30 to 900 °C at a heating rate of 10 °C min^{-1} in air.

2.5. Electrochemical measurements

The electrochemical properties of the mesoporous Co_3O_4@graphene in LIBs were evaluated by a galvanostatic charge/discharge technique. The mass loading of these integrated electrodes was 1–3 mg cm^{-2}, the current density and capacity are normalized on the total mass of the electrodes. A Co_3O_4 electrode was prepared by mixing 80 wt% active material, 10 wt% conductive carbon black (super P) as a conducting additive and 10 wt% polyvinylidene fluoride dissolved in N-methyl-2-pyrrolidone as a binder, and the capacity is normalized on the mass of Co_3O_4. Coin cells were assembled in an argon-filled glove box, the samples as test electrode with metallic lithium as the counter/reference electrode, 1 M $LiPF_6$ in ethylene carbonate and dimethyl carbonate (1:1 vol) as the electrolyte, and Celgard 2400 polypropylene as the separator. Charge-discharge measurements were carried out galvanostatically at various current densities over a voltage range of 0.001–3 V (*vs.* Li/Li^+) using a battery testing system (LAND CT2001A). Cyclic voltammogram (CV) measurements were carried out using a VSP-300 multichannel potentiostat/galvanostat (Bio-Logic, France) workstation in the voltage range of 0.001–3.0 V (*vs.* Li^+/Li) at a scan rate of 0.2 mV s^{-1}. Electrochemical impedance spectroscopy (EIS) measurements were carried out by applying a perturbation voltage of 10 mV in a frequency range of 100 kHz to 10 mHz.

3. Results and discussion

The morphology and microstructure of the nanostructured Co_3O_4@graphene membrane are shown in Fig. 2. It can be seen that the electrode is flexible and can be bent into arbitrary shapes (Fig. 2a). The graphene membrane was grey with some metallic sheen. During the hydrothermal reaction, the bottom surface (contact with the reaction solution) of the graphene membrane turned to black owing to the growth of Co_3O_4, while the top surface preserved the original morphology after hydrothermal reaction and subsequent thermal treatment (Supporting Information, Fig. S1). Fig. 2b–d presents SEM images of the corresponding nanostructured Co_3O_4@graphene membrane, which were obtained under different reaction times followed by the same thermal annealing. It could be observed that Co_3O_4 nanowires, which have an average diameter of 100 nm and length around 2–5 um, distribute uniformly and cover the whole graphene membrane after 4 h. It is noted that the structure and morphology of Co_3O_4 changed gradually with extending the reaction time. When the reaction time reaches 10 h, Co_3O_4 nanowalls begin to appear among these nanowires (Fig. 2c). When prolonging the reaction time to 24 h, it can be seen that the nanowalls with a height and thickness around 3–5 um and 100 nm, respectively, replace nanowires and cover the whole substrate (Fig. 2d). The crystallinity and phase purity of nanostructured Co_3O_4@graphene membrane were confirmed by XRD as shown in Supporting Information, Fig. S2. Because the graphene material was obtained through intercalation exfoliation method, the crystallization of the few-layer graphene is very good, and the diffraction peaks of graphene at around 26 and 54° are obvious. The other identified peaks can be assigned to Co_3O_4 (JCPDS No. 43-1003) and no peaks of impurities were observed, indicating the high purity of the samples [30]. The Co_3O_4 contents in the samples with

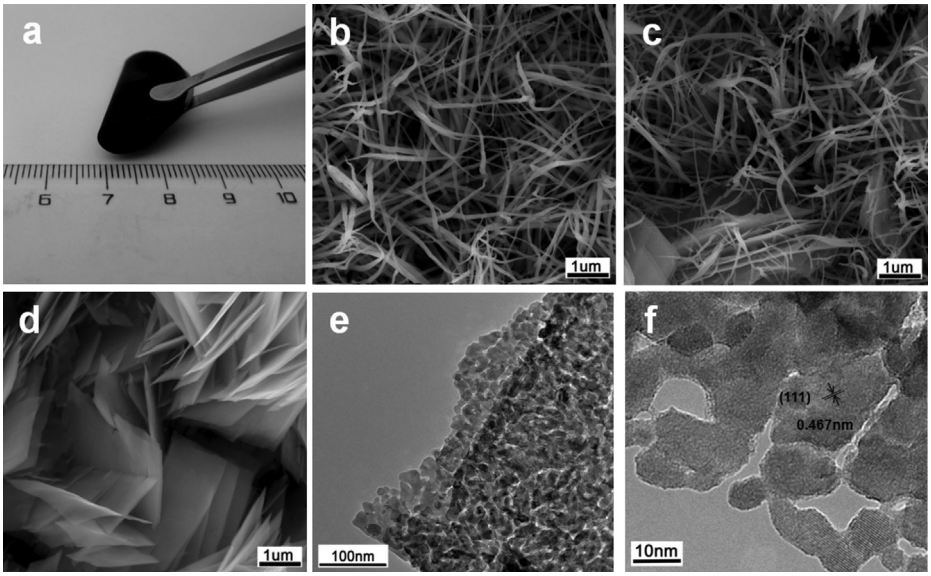

Fig. 2. (a) Photograph of a flexible nanostructured Co_3O_4@graphene membrane. (b–d) SEM images of the nanostructured Co_3O_4@graphene membrane after hydrothermal reaction for 4 h, 10 h and 24 h and undergoing the subsequent same heat treatment, respectively. (e, f) TEM images of Co_3O_4 nanowall@graphene membrane at different magnifications.

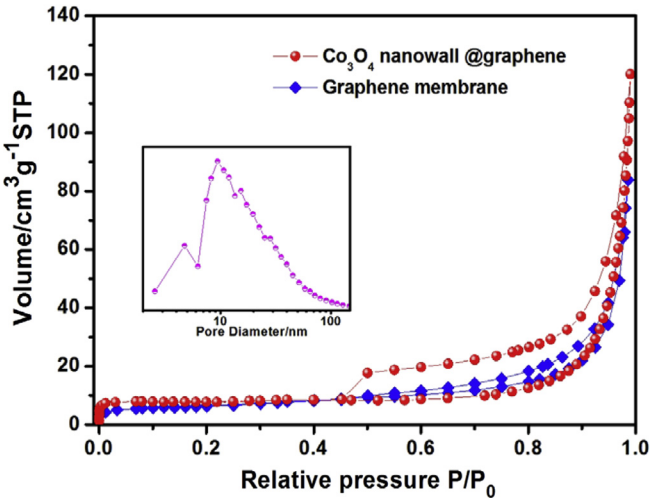

Fig. 3. N_2 adsorption/desorption isotherms of Co_3O_4 nanowall@graphene membrane and graphene membrane, inset: pore size distribution of Co_3O_4 nanowall@graphene membrane.

different reaction time are 21, 35 and 52 wt% according to TG analysis as shown in Supporting Information, Fig. S3.

During the reaction, small nanoparticles will assemble together, so as to gradually form a discrete polycrystalline structure from Co_3O_4 nanowires to Co_3O_4 nanowalls. It is clear from a typical TEM image (Fig. 2e) that an individual nanowall appears to be composed of small nanoparticles, showing a highly porous structure. From the Fig. 2f, the pore size of Co_3O_4 nanowalls is about 5–10 nm, and the adjacent fringe spacing of the aligned lattice fringes is about 0.467 nm, corresponding to the (111) plane of Co_3O_4. In contrast, without graphene membrane as the substrate, the nanowalls aggregated, while the porous structure still maintained (Supporting Information, Fig. S4). The porous structure characteristics and Brunauer–Emmett–Teller (BET) specific surface area of the Co_3O_4 nanowall@graphene membrane and the graphene membrane were investigated by nitrogen isothermal adsorption in Fig. 3. The BET surface area of the Co_3O_4 nanowall@graphene membrane (35 $m^2\ g^{-1}$) is higher than the graphene membrane (22 $m^2\ g^{-1}$). Owing to the Co_3O_4 nanowall growth, the existence of mesopores was obviously observed in the N_2 desorption isotherm. The pore size distribution indicates that the main pore size (inset in Fig. 3) in the Co_3O_4 nanowall@graphene membrane is around 10 nm, which corresponding to the TEM observation (Fig. 2f).

The electrochemical performance of electrodes was closely related to their structure and morphology. To identify the electrochemical reactions, CV measurement was carried out in the range of 0.001–3.0 V for five cycles at a scan rate of 0.2 mV s^{-1}. In the first discharge process (Fig. 4a), the first small cathodic peak of the Co_3O_4 nanowall@graphene membrane was observed around 1.1 V corresponding to the reduction of Co_3O_4. The obvious cathodic peak was located at around 0.75 V, which was attributed to the electrochemical reduction of Co_3O_4 to metallic cobalt accompanying the formation of Li_2O and the solid electrolyte interphase (SEI) film [16,31]. In the anodic process, broad peaks located at around 2.15 V and 2.5 V can be ascribed to the reversible oxidation reaction from cobalt to Co_3O_4, which is a multi-step reaction process [32]. The total electrochemical reaction mechanism of Co_3O_4 anode can be described by the following electrochemical conversion reaction: [17]

$$Co_3O_4 + 8Li^+ + 8e^- \Leftrightarrow 4Li_2O + 3Co$$

Both Co_3O_4 and graphene are able to react with lithium ions for reversible lithium storage. There was an obvious reduction peak at 0.01 V, which indicates lithium insertion in graphene membrane, while the peak located at around 0.21 V during the anodic process corresponds to lithium extraction from graphene membrane [18]. From the second cycle, the main cathodic peak shifted to a higher potential at about 0.83 V while the oxidation peak position remains almost unchanged and CV curves exhibit similar shapes, indicating the good reversibility of lithium storage. In contrast, the Co_3O_4 electrode exhibits a pair of asymmetric redox peaks in the first cycle, and from the second cycle the cathodic peaks shifted to lower potential accompanying with the decrease of the peak intensity and integral areas, suggesting the poor irreversible reactions (Fig. 4b). On the one hand, the poor CV performance of the pure Co_3O_4 is due to the relatively low calcination temperature. On the other hand, serious agglomeration and pulverization of Co_3O_4 electrode during cycling lead to the fast capacity fading, which will be confirmed in the following discussion.

The first charge–discharge profiles of the graphene membrane, Co_3O_4, Co_3O_4 nanowire@graphene membrane and Co_3O_4 nanowall@graphene membrane between 0.001 and 3.0 V at a current density of 100 mA g^{-1} are shown in Fig. 5a. An extended voltage plateau at around 1.1 V was observed for the Co_3O_4, Co_3O_4 nanowire@graphene membrane and Co_3O_4 nanowall@graphene membrane, resulting from the lithium reaction with Co_3O_4 and the formation of Co and Li_2O [33]. In the charge curves, the sloped region from 1.5 to 2.2 V corresponds to the reversible oxidation of Co_3O_4. On the other hand, the charge curve of Co_3O_4 was a straight uptrend line, which is in agreement with the CV analysis (Fig. 4). The Columbic efficiency of Co_3O_4 nanowire@graphene membrane (68%) and Co_3O_4 nanowall@graphene membrane (71%) is much

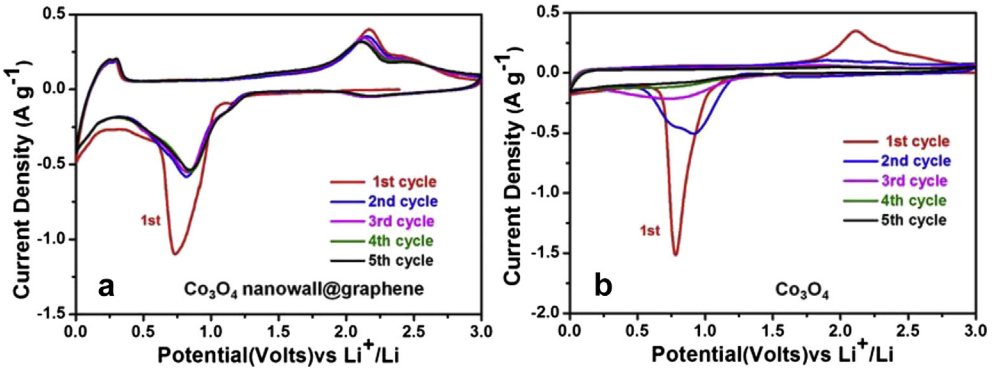

Fig. 4. CVs of the (a) Co_3O_4 nanowall@graphene membrane and (b) Co_3O_4 at a scan rate of 0.2 mV s^{-1} for five cycles.

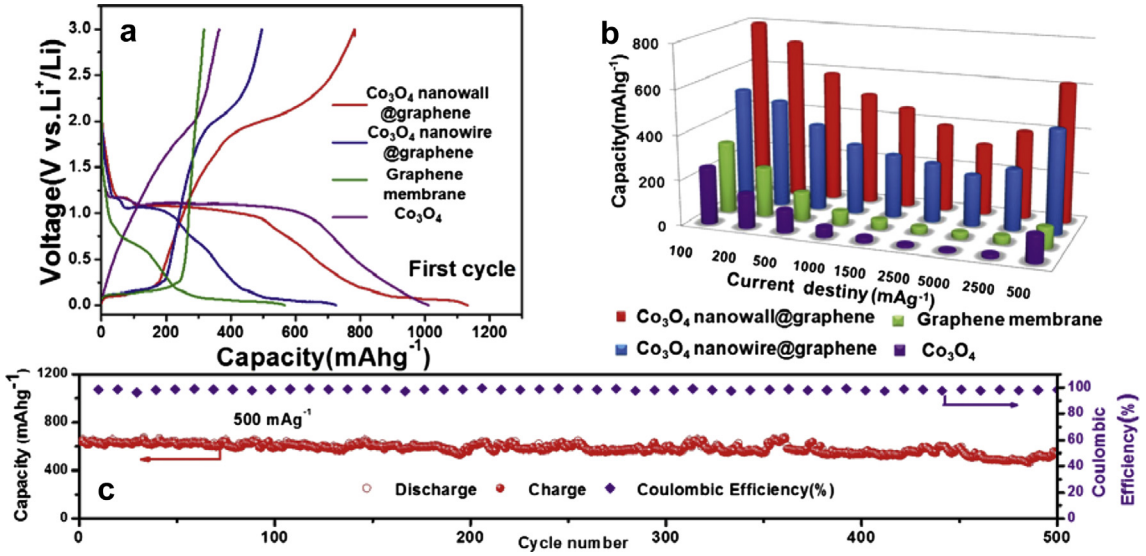

Fig. 5. (a) First galvanostatic charge–discharge curves of the graphene membrane, Co_3O_4, Co_3O_4 nanowire@graphene membrane and Co_3O_4 nanowall@graphene membrane at a current density of 100 mA g^{-1}. (b) Rate capacity of the Co3O4 nanowall@graphene membrane, Co_3O_4 nanowire@graphene membrane, graphene membrane and Co_3O_4 at different current densities (the rate capacity was measured at five points in each current density and then took the average). (c) Cyclic performance of Co_3O_4 nanowall@graphene membrane at a current density of 500 mA g^{-1} after the rate capability test for 500 cycles.

higher than that of Co_3O_4 (36%) and graphene membrane (56.3%). The irreversible capacity loss can be attributed to the decomposition of electrolyte and the formation of a SEI film [34,35]. The rate performance, which is one of the most critical parameters with regard to LIBs applications, of the materials was also investigated as shown in Fig. 5b and Fig. S5. Compared to other samples, the Co_3O_4 nanowall@graphene membrane delivered the highest reversible capacity of around 800 mA h g^{-1} at a current density of 100 mA g^{-1}. With the increase of current density to 5000 mA g^{-1}, the specific capacity still retained 320 mA h g^{-1}, demonstrating a magnificent high rate performance. The cyclic stability of the samples was investigated at a current density of 500 mA g^{-1} after the rate capability test, as shown in Fig. 5c. The Co_3O_4 nanowall@graphene electrode demonstrated excellent cyclic stability above

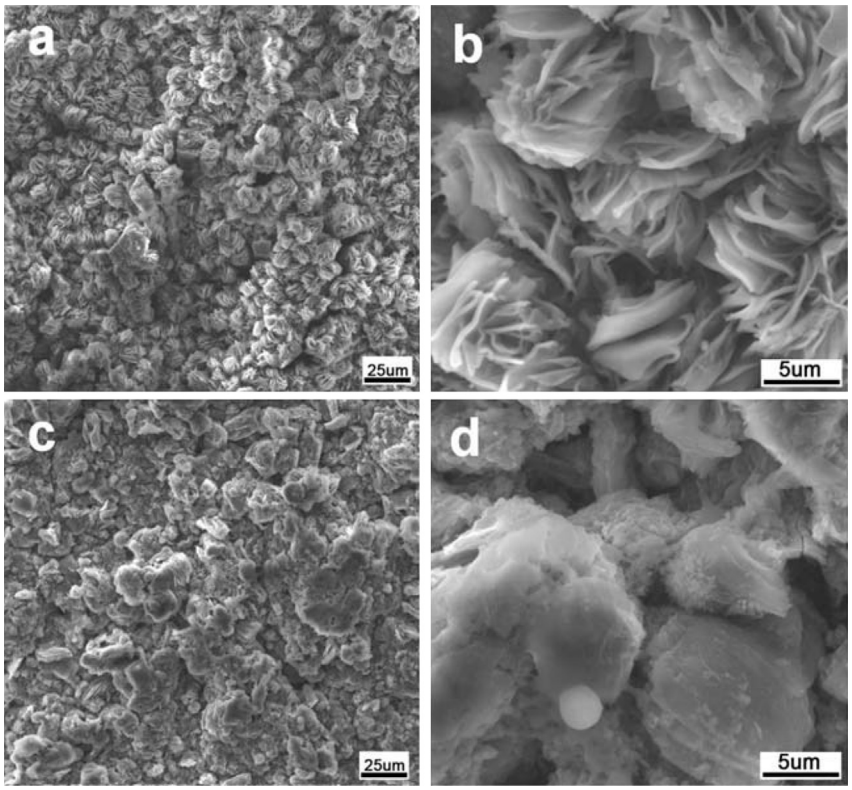

Fig. 6. SEM images of the (a, b) Co_3O_4 nanowall@graphene composite and (c, d) Co_3O_4 after 500 discharge/charge cycles.

600 mA h g^{-1} without any capacity loss and a Coulombic efficiency close to 100% over 500 cycles. The electrochemical performance is comparable with most state-of-the-art Co_3O_4 electrode materials that use metallic current collector and conductive additive [16,36,37].

To understand the long-life performance of the nanostructured Co_3O_4 nanowall@graphene electrode, the Co_3O_4 nanowall@graphene composite and Co_3O_4 electrodes after 500 cycles were taken out from the coin cells, washed using a dimethyl carbonate solution, and the morphology of the samples was observed by SEM. As shown in Fig. 6a, b, no obvious changes in the morphology are observed for the Co_3O_4 nanowall@graphene composite, in which the Co_3O_4 nanowalls were still tightly adhered to the graphene membrane, demonstrating the structure integrity of the composite upon electrochemical cycling. In contrast, the serious agglomeration and cracks can be observed in Co_3O_4 electrode (Fig. 6c, d), indicating the structural evolution and aggregation of Co_3O_4 during cycling that leads to the fast capacity fading. The structural stability of the composite can be ascribed to the directly grown structure that tightly connects the graphene membrane with Co_3O_4, preventing the detachment and agglomeration of Co_3O_4 nanowalls during cycling, which contributes to the excellent cyclic stability.

To prove whether the Co_3O_4 nanowall@graphene composite could improve the transport kinetics of electrons and ions, EIS measurements were carried out, as shown in Fig. 7. The Nyquist plots of the Co_3O_4 nanowall@graphene composite and Co_3O_4 electrodes are similar with a typical semicircle in the high-medium frequency region and an inclined line at low frequency region, which can be ascribed to the charge-transfer resistance R_{ct} and a mass-transfer process [38,39]. The value of R_{ct} for the Co_3O_4 nanowall@graphene composite (287 Ω) is much smaller than that of the Co_3O_4 electrode with a value of 770 Ω, implying that the Co_3O_4 nanowall@graphene composite electrode exhibits faster charge-transfer and has smaller electrochemical reaction resistance compared to that of the Co_3O_4 electrode. The direct growth of Co_3O_4 nanowall on the surface of graphene membrane enables good adhesion between Co_3O_4 and the current collector, leads to a decrease in the contact resistance, thus lowering the charge-transfer impedance. It can be seen that the low frequency tail for the two samples were also different, which represents the electrolyte ion diffusion behaviour in the electrode materials [35,40,41]. The steeper low frequency tail of Co_3O_4 nanowall@graphene electrode indicates lower ion diffusion resistance compared to Co_3O_4 electrode. As expected, it indicates that Co_3O_4 nanowall@graphene composite electrode possesses a high electrical conductivity, a rapid charge transfer process and good lithium ion reaction kinetics, promoting the improved electrochemical performance of the composite.

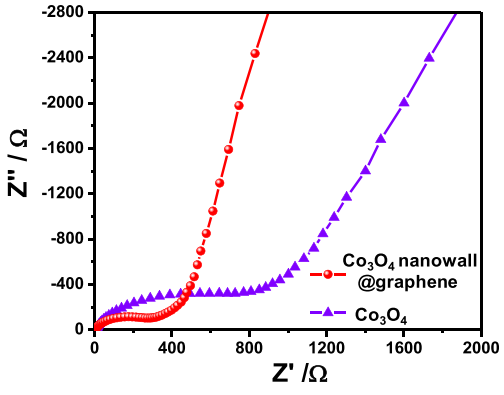

Fig. 7. Nyquist plots of the Co_3O_4 nanowall@graphene composite and Co_3O_4 electrodes measured from 10 kHz to 10 mHz at room temperature.

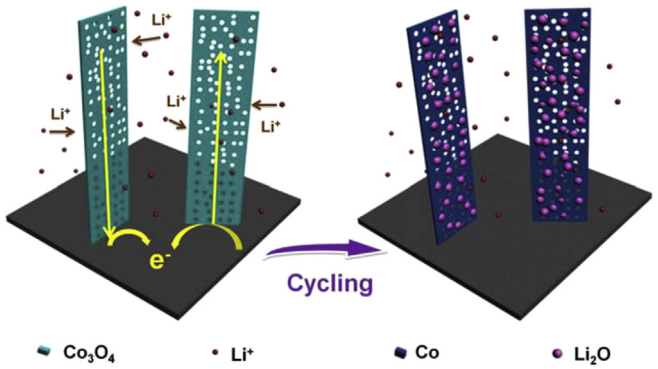

Fig. 8. Schematic of the electrochemical reaction during cycling process between lithium and a Co_3O_4 nanowall grown on the graphene membrane.

All in all, the high performance is attributed to the unique morphology and structural characteristic of the electrodes. The areal density of the graphene membrane is 1–1.5 mg cm^{-2}, which is less than 88%–92% that of the Cu foil (13.4 mg cm^{-2}). And binder also accounts for approximately 2–5% of the weight of a typical conventional cell. Owing to the use of the lighter graphene membrane replacing that of Cu foil and no use of conductive additive and binder in the fabrication of the above electrodes, the weight of the battery reduces about 6%–8%, and the capacity was normalized on the total mass of the electrodes, consequently the energy density of the battery can be greatly improved [12,42]. Due to the direct growth on the current collector (Fig. 8), good contact and strong binding between Co_3O_4 and graphene membrane can be obtained, which facilitates electron transport from the graphene to Co_3O_4 nanowalls. The mesoporous Co_3O_4 nanowalls can provide more interface with large active sites for Li^+ insertion [43]. The porous nanostructure is beneficial to the electrolyte diffusion, provides fast transport channels for Li ions, and accommodates the strain of volume change during the continuous lithiation and delithiation processes [22,44].

4. Conclusion

In summary, we fabricated mesoporous Co_3O_4 with controllable structures directly grown on a graphene membrane by hydrothermal reaction followed by annealing treatment. The light graphene current collector with high electrical conductivity and stability contributes to the high energy density of the LIBs. A mesoporous structure with enough space is beneficial to lithium ion transport and strain buffer of Co_3O_4 during lithiation/delithiation, rendering the electrodes high performance. Specially, the Co_3O_4 nanowall@graphene membrane shows excellent cyclic stability without capacity loss over 500 cycles under a high current density of 500 mA g^{-1}. This novel structure paves the way to design electrodes for high performance LIBs.

Acknowledgements

This work was supported by the Key Research Program of Ministry of Science and Technology, China (Nos. 2014CB932402 and 2012AA030303), the National Science Foundation of China (Nos. 51221264, 51172239 and 51372253), and the " Strategic Priority Research Program" of the Chinese Academy of Sciences (No. XDA01020304).

Appendix A. Supplementary data

Supplementary data related to this article can be found at http://dx.doi.org/10.1016/j.jpowsour.2013.12.129.

References

[1] M. Armand, J.M. Tarascon, Nature 451 (2008) 652–657.
[2] C. Liu, F. Li, L.-P. Ma, H.-M. Cheng, Adv. Mater. 22 (2010) E28–E62.
[3] P.G. Bruce, S.A. Freunberger, L.J. Hardwick, J.-M. Tarascon, Nat. Mater. 11 (2012) 19–29.
[4] G.M. Zhou, L.-C. Yin, D.-W. Wang, L. Li, S. Pei, I.R. Gentle, F. Li, H.-M. Cheng, ACS Nano 7 (2013) 5367–5375.
[5] S. Luo, K. Wang, J. Wang, K. Jiang, Q. Li, S. Fan, Adv. Mater. 24 (2012) 2294–2298.
[6] A. Marschilok, C.-Y. Lee, A. Subramanian, K.J. Takeuchi, E.S. Takeuchi, Energy Environ. Sci. 4 (2011) 2943–2951.
[7] P.L. Taberna, S. Mitra, P. Poizot, P. Simon, J.M. Tarascon, Nat. Mater. 5 (2006) 567–573.
[8] K. Wang, S. Luo, Y. Wu, X. He, F. Zhao, J. Wang, K. Jiang, S. Fan, Adv. Funct. Mater. 23 (2013) 846–853.
[9] J.W. Braithwaite, A. Gonzales, G. Nagasubramanian, S.J. Lucero, D.E. Peebles, J.A. Ohlhausen, W.R. Cieslak, J. Electrochem. Soc. 146 (1999) 448–456.
[10] L. Hu, H. Wu, F. La Mantia, Y. Yang, Y. Cui, ACS Nano 4 (2010) 5843–5848.
[11] G.M. Zhou, L. Li, Q. Zhang, N. Li, F. Li, Phys. Chem. Chem. Phys. 15 (2013) 5582–5587.
[12] L.-F. Cui, L. Hu, J.W. Choi, Y. Cui, ACS Nano 4 (2010) 3671–3678.
[13] B. Liu, J. Zhang, X. Wang, G. Chen, D. Chen, C. Zhou, G. Shen, Nano Lett. 12 (2012) 3005–3011.
[14] N. Li, Z. Chen, W. Ren, F. Li, H.-M. Cheng, Proc. Natl. Acad. Sci. U. S. A. 109 (2012) 17360–17365.
[15] H. Gwon, H.S. Kim, K.U. Lee, D.H. Seo, Y.C. Park, Y.S. Lee, B.T. Ahn, K. Kang, Energy Environ. Sci. 4 (2011) 1277–1283.
[16] Z.-S. Wu, W. Ren, L. Wen, L. Gao, J. Zhao, Z. Chen, G. Zhou, F. Li, H.-M. Cheng, ACS Nano 4 (2010) 3187–3194.
[17] W.Y. Li, L.N. Xu, J. Chen, Adv. Funct. Mater. 15 (2005) 851–857.
[18] J. Yao, X.P. Shen, B. Wang, H.K. Liu, G.X. Wang, Electrochem. Commun. 11 (2009) 1849–1852.
[19] Z. Zhang, J. Hao, W. Yang, B. Lu, X. Ke, B. Zhang, J. Tang, ACS Appl. Mater. Interfaces 5 (2013) 3809–3815.
[20] L. Tao, J. Zai, K. Wang, H. Zhang, M. Xu, J. Shen, Y. Su, X. Qian, J. Power Sources 202 (2012) 230–235.
[21] Y. Li, B. Tan, Y. Wu, J. Am. Ceram. Soc. 128 (2006) 14258–14259.
[22] X.-Y. Xue, S. Yuan, L.-L. Xing, Z.-H. Chen, B. He, Y.-J. Chen, Chem. Commun. 47 (2011) 4718–4720.
[23] X.W. Lou, D. Deng, J.Y. Lee, J. Feng, L.A. Archer, Adv. Mater. 20 (2008) 258–262.
[24] J. Chen, X.-H. Xia, J.-P. Tu, Q.-Q. Xiong, Y.-X. Yu, X.-L. Wang, C.-D. Gu, J. Mater. Chem. 22 (2012) 15056–15061.
[25] X.Y. Feng, C. Shen, Y. Yu, S.Q. Wei, C.H. Chen, J. Power Sources 230 (2013) 59–65.
[26] D. Liu, X. Wang, X. Wang, W. Tian, Y. Bando, D. Golberg, Sci. Rep. 3 (2013).
[27] Y. Xiao, C. Hu, M. Cao, J. Power Sources 247 (2014) 49–56.
[28] G.M. Zhou, S. Pei, L. Li, D.-W. Wang, S. Wang, K. Huang, L.-C. Yin, F. Li, H.-M. Cheng, Adv. Mater. (2013), http://dx.doi.org/10.1002/adma.201302877.
[29] S. Park, R.S. Ruoff, Nat. Nanotechnol. 4 (2009) 217–224.
[30] G. Yang, D. Gao, J. Zhang, J. Zhang, Z. Shi, Z. Zhu, D. Xue, RSC Adv. 3 (2013) 508–512.
[31] L. Zhuo, Y. Wu, J. Ming, L. Wang, Y. Yu, X. Zhang, F. Zhao, J. Mater. Chem. A 1 (2013) 1141–1147.
[32] N. Jayaprakash, W.D. Jones, S.S. Moganty, L.A. Archer, J. Power Sources 200 (2012) 53–58.
[33] Y. Li, B. Tan, Y. Wu, Nano Lett. 8 (2007) 265–270.
[34] W. Yao, J. Yang, J. Wang, Y. Nuli, J. Electrochem. Soc. 155 (2008) A903–A908.
[35] B.G. Choi, S.-J. Chang, Y.B. Lee, J.S. Bae, H.J. Kim, Y.S. Huh, Nanoscale 4 (2012) 5924–5930.
[36] X. Yang, K. Fan, Y. Zhu, J. Shen, X. Jiang, P. Zhao, C. Li, J. Mater. Chem. 22 (2012) 17278–17283.
[37] B. Li, H. Cao, J. Shao, G. Li, M. Qu, G. Yin, Inorg. Chem. 50 (2011) 1628–1632.
[38] G.M. Zhou, D.-W. Wang, L. Li, N. Li, F. Li, H.-M. Cheng, Nanoscale 5 (2013) 1576–1582.
[39] M.V. Reddy, T. Yu, C.H. Sow, Z.X. Shen, C.T. Lim, G.V. Subba Rao, B.V.R. Chowdari, Adv. Funct. Mater. 17 (2007) 2792–2799.
[40] T. Doi, Y. Iriyama, T. Abe, Z. Ogumi, Anal. Chem. 77 (2005) 1696–1700.
[41] G.M. Zhou, D.-W. Wang, L.-C. Yin, N. Li, F. Li, H.-M. Cheng, ACS Nano 6 (2012) 3214–3223.
[42] L. Gaines, R. Cuenca, Argon National Laboratory: Argonne, IL, 2000.
[43] X.W. Lou, D. Deng, J.Y. Lee, L.A. Archer, J. Mater. Chem. 18 (2008) 4397–4401.
[44] M.M. Rahman, J.-Z. Wang, M.F. Hassan, S. Chou, Z. Chen, H.K. Liu, Energy Environ. Sci. 4 (2011) 952–957.